DALTON
FULL PAPER

A kinetically inert and optically active Cr^{III} partner in thermodynamically self-assembled heterodimetallic non-covalent d–f podates †

Martine Cantuel,[a] Gérald Bernardinelli,[b] Daniel Imbert,[c] Jean-Claude G. Bünzli,[c] Gérard Hopfgartner[d] and Claude Piguet*[a]

[a] *Department of Inorganic, Analytical and Applied Chemistry, University of Geneva, 30 quai E. Ansermet, CH-1211 Geneva 4, Switzerland. E-mail: Claude.Piguet@chiam.unige.ch*
[b] *Laboratory of X-ray Crystallography, 24 quai E. Ansermet, CH-1211 Geneva 4, Switzerland*
[c] *Swiss Federal Institute of Technology Lausanne, Institute of Molecular and Biological Chemistry, BCH 1402, CH-1015 Lausanne, Switzerland*
[d] *F. Hoffmann-La Roche Ltd, Pharmaceuticals Division, PRNS 68/142, CH-4070 Basle, Switzerland and Department of Pharmacy, University of Geneva, 30 quai E. Ansermet, CH-1211 Geneva 4, Switzerland*

Received 3rd January 2002, Accepted 12th February 2002
First published as an Advance Article on the web 10th April 2002

Stoichiometric mixing of the segmental ligand 2-{6-[*N*,*N*-diethylcarboxamido]pyridin-2-yl}-1,1′-dimethyl-5,5′-methylene-2′-(5-methylpyridin-2-yl)bis[1H-benzimidazole] (L) with $Ln(CF_3SO_3)_3$ (Ln = La–Lu) and $Cr(CF_3SO_3)_2$ under an inert atmosphere produces quantitatively the self-assembled triple-stranded non-covalent podates (HHH)-$[LnCr^{II}L_3]^{5+}$. Air oxidation of the low-spin Cr^{II} complexes gives selectively the head-to-head-to-head podates (HHH)-$[LnCr^{III}L_3]^{6+}$ into which inert Cr^{III} has been incorporated. The X-ray crystal structures of $[LnCr^{III}(L)_3](CF_3SO_3)_6(CH_3CN)_4$ (Ln = Eu, **7**; Ln = Lu, **8**) confirm the formation of regular triple-helical cations (HHH)-$[LnCr^{III}L_3]^{6+}$ whose structure is maintained in acetonitrile according to ESI–MS, spectrophotometry and NMR data. Photophysical studies evidence efficient sensitization of both Eu^{III} and Cr^{III} through ligand excitation at low temperature, while a subsequent intramolecular $Eu^{III} \longrightarrow Cr^{III}$ energy transfer ($\eta = 70\%$) limits Eu-centred luminescence and induces directional light-conversion along the three-fold axis, resulting in Cr^{III} emission. For (HHH)-$[TbCr^{III}L_3]^{6+}$, the better spectral overlap between the emission spectrum of Tb^{III} ($^5D_4 \longrightarrow {}^7F_J$) and the absorption spectrum of Cr^{III} ($^4A_2 \longrightarrow {}^4T_2$) provides a quantitative $Tb^{III} \longrightarrow Cr^{III}$ energy transfer ($\eta \geq 99\%$) and long-range intermetallic communication. De-complexation of Ln^{III} with water or $EDTA^{4-}$ gives the first inert and optically active-Cr^{III}-containing triple-helical nonadentate receptor (HHH)-$[Cr^{III}L_3]^{3+}$.

Introduction

The peculiar orbitally non-degenerate quartet ground state corresponding to the open-shell $(t_{2g})^3$ electronic configuration of octahedral Cr^{III} ($^4A_{2g}$ in O_h symmetry), combined with the high charge (3+) borne by the cation provide exceptional kinetic inertness and structural rigidity to Cr^{III} complexes (the rate of water exchange in $[Cr(OH_2)_6]^{3+}$ amounts to $k_{(298\ K)} = 2.4 \times 10^{-6}\ s^{-1}$).[1] A huge number of pseudo-octahedral Cr^{III} complexes with well-defined geometries were isolated during the early seventies with the main goal of refining theoretical inorganic electronic spectroscopy,[2] but recent attempts to design sophisticated heteropolymetallic assemblies with new optical and magnetic properties have resorted to kinetically inert Cr^{III}-containing building blocks.[3–6] For instance, tris-oxalato ($[Cr(ox)_3]^{3-}$),[3] mixed oxalato-acetylacetonato ($[Cr(ox)(acac)_2]^-$)[4] and oxalato-bipyridine ($[Cr(ox)_2(bipy)]^-$)[5] complexes have been successfully used as precursors for preparing discrete[4,5] or infinite[3] polymetallic d–d or d–f assemblies, while inert {(TACN)Cr} units (TACN = 1,4,7-trimethyl-1,4,7-triazacyclononane) have been designed for the capping of metallo-supramolecular cryptands containing highly labile d-block ions (M = Mn^{II}, Ni^{II}, Cu^{II}).[6]

From the point of view of electronic structures and optical properties, Cr^{III} is a fascinating partner because its first excited state, ^2E_g, is poorly sensitive to crystal-field effects ($(t_{2g})^3$ electronic configuration), but it possesses a spin multiplicity different from that of the ground state ($^4A_{2g}$), thus leading to long-lived luminescence at low temperature with only minor Stokes shifts.[7] On the other hand, the first spin-allowed transition to the $^4T_{2g}$ state ($(t_{2g})^2e_g$ configuration) is very sensitive to ligand-field effects and the relative energies of the excited $^4T_{2g}$ and ^2E_g states can be tuned by judicious ligand design and/or by the application of external pressure.[8] Potential overlap of the Cr^{III}-centred emission bands $^4T_{2g} \longrightarrow {}^4A_{2g}$ and $^2E_g \longrightarrow {}^4A_{2g}$ with 4f $\longrightarrow$ 4f absorptions bands of several lanthanide ions has prompted the systematic introduction of Cr^{III} as donor in weak-field garnets (Al_2O_3) for sensitizing near-IR emitters (Nd^{III}, Er^{III} and Tm^{III}) *via* energy transfer processes. For strong-field ligands, the spin-allowed $^4A_{2g} \longrightarrow {}^4T_{2g}$ and $^4A_{2g} \longrightarrow {}^4T_{1g}$ (F and P) transitions arise in the visible or near-UV domain and may overlap with emission bands of Ln^{III} possessing a large energy gap (Ln = Eu, Tb) leading to efficient multipolar $Ln^{III} \longrightarrow Cr^{III}$ energy

† Electronic supplementary information available (ESI): tables of molecular peaks obtained by ESI-MS (Table S1), elemental analyses (Table S2), least-squares plane and structural data for $[LnCr^{III}(L)_3](CF_3SO_3)_6(CH_3CN)_4$ (Ln = Eu, **7**; Ln = Lu, **8**; Tables S3–S7), geometrical analysis of the triple helix (Table S8), integrated emission intensities (Table S9); figures showing projection of the unit cell of **8** (Fig. S1), superposition of the molecular structures of **7** and **8** (Fig. S2) and emission spectra and lifetimes for GdCr and TbCr complexes (Fig. S3–S5). See http://www.rsc.org/suppdata/dt/b2/b200011c/

transfers in which Cr^{III} acts as an acceptor.[9] The combination of spectroscopically active Ln^{III} ions with Cr^{III} thus opens new perspectives for directional light-conversion in organized discrete self-assembled metallosupramolecular architectures provided that kinetic inertness is overcome during the complete exploration of the energy hypersurface leading to the thermodynamically most stable, defect-free and self-healing assembly.[10]

Preliminary investigations along this line relied upon mixing the segmental ligand L with labile Co^{II} and Ln^{III} ions to give quantitatively the C_3-symmetrical (HHH)-$[LnCo^{II}L_3]^{5+}$ non-covalent podates. Oxidative post-modification produced (HHH)-$[LnCo^{III}L_3]^{6+}$ with d^6 low-spin Co^{III} (Fig. 1).[11] However,

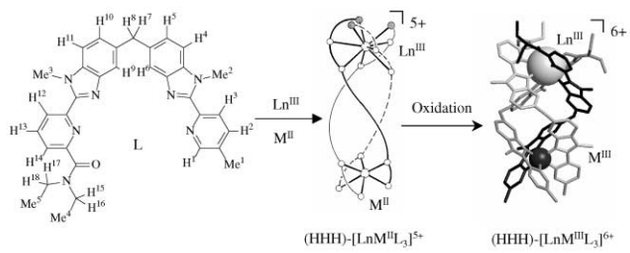

Fig. 1 Self-assembly with oxidative post-modification of the inert non-covalent podates (HHH)-$[LnM^{III}L_3]^{6+}$ in acetonitrile (M = Cr, Co).

subsequent removal of Ln^{III} failed to give the kinetically inert (HHH)-$[Co^{III}L_3]^{3+}$ receptors and 'rapid' isomerisation processes occurred within hours (probably catalysed by traces of Co^{II}).[11] A similar approach can be envisioned for Cr^{III} because the reduced Cr^{II} analogue is expected to be highly labile (the rate of methanol exchange in $[Cr(CH_3OH)_6]^{2+}$ amounts to $k_{(298\ K)} = 1.2 \times 10^8\ s^{-1}$),[12] and electrochemically accessible when complexed to heterocyclic nitrogen atoms in polar solvents ($E^o([Cr(bipy)_3]^{3+}/[Cr(bipy)_3]^{2+}) = -0.25$ V *vs.* NHE; bipy = 2,2′-bipyridine).[13] Moreover, this negative reduction potential prevents the formation of a significant amount of Cr^{II} in solution, a crucial point if kinetically inert Cr^{III}-complexes are considered. In this paper, we report on the selective formation of the inert non-covalent podates (HHH)-$[LnCr^{III}L_3]^{6+}$ obtained by thermodynamic self-assembly of (HHH)-$[LnCr^{II}L_3]^{5+}$ followed by air oxidation in acetonitrile. Particular attention is focused on (i) the intramolecular intermetallic energy transfer processes responsible for directional light-conversion within the $LnCr^{III}$ complexes and (ii) the exceptional inertness of the (HHH)-$[CrL_3]^{3+}$ tripod which prevents isomerisation over a period of months.

Results and discussion

Thermodynamic self-assembly of $[LnCr^{II}L_3]^{5+}$ (Ln = La, Eu, Gd, Tb, Tm, Lu)

Stoichiometric mixing of L (3 equiv.), $Cr(CF_3SO_3)_2 \cdot 13H_2O$ (1 equiv.) and $Ln(CF_3SO_3)_3 \cdot nH_2O$ (1 equiv., n = 3–6, Ln = La, Eu, Gd, Tb, Tm, Lu) in degassed acetonitrile provides deep green solutions whose absorption spectra are diagnostic for low-spin Cr^{II} in trigonally distorted pseudo-octahedral environments constituted of three wrapped bidentate heterocyclic α,α′-di-imine ligands (Table 1, Fig. 2).[14,15] The two intense transitions at low energies can be assigned to LMCT by comparison with those found for $[Cr(bipy)_3]^{2+}$ in methanol (8700 cm^{-1} (ε = 10000 $M^{-1}\ cm^{-1}$) and 9900 cm^{-1} (ε = 2900 $M^{-1}\ cm^{-1}$)).[14] The series of poorly resolved bands in the range 11000–24000 cm^{-1} correspond to overlapping d–d transitions possessing significant CT character and whose tentative assignments are given in Table 1.[14] Compared to $[Cr(bipy)_3]^{2+}$,[14] the Cr^{II}-centred d–d transitions in (HHH)-$[LnCrL_3]^{2+}$ are of similar intensities, but are systematically shifted toward lower energies in agreement with the weaker ligand field produced by bidentate pyridylbenzimidazole (pybzim) binding units (10Dq =

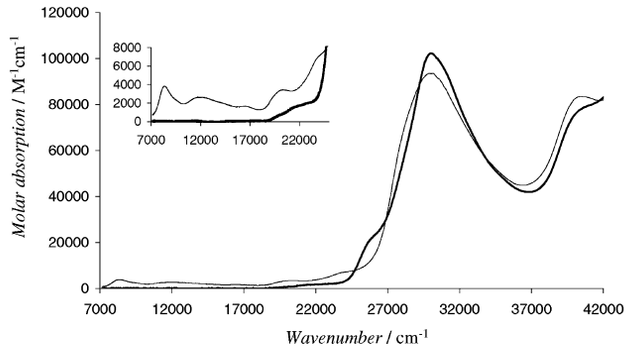

Fig. 2 Absorption spectra of (HHH)-$[LaCr^{II}L_3]^{5+}$ (2.3×10^{-3} mol dm^{-3}, thin trace) and (HHH)-$[LaCr^{III}L_3]^{6+}$ (10^{-3} mol dm^{-3}, bold trace) in acetonitrile at 293 K.

17370 cm^{-1} in $[Cr(bipy)_3]^{2+}$ and 10Dq = 16000 cm^{-1} in $[Cr(pybzim)_3]^{2+}$).[15] The intense band in the UV can be ascribed to ligand-centred π ⟶ π* transitions which are altered by complexation of the bidentate and tridentate segments of L to Cr^{II} and Ln^{III} respectively, as previously discussed for (HHH)-$[LnZnL_3]^{5+}$,[16] (HHH)-$[LnFeL_3]^{5+}$ [17] and (HHH)-$[LnCoL_3]^{5/6+}$.[11] We conclude that low-spin Cr^{II} is coordinated by three bidentate pyridylbenzimidazole segments in a trigonally-distorted pseudo-octahedral arrangement.

The ^{1}H NMR spectra of (HHH)-$[LnCrL_3]^{2+}$ (Ln = La, Lu) show 20 broadened signals spread over 50 ppm and corresponding to three equivalent ligands L related by a three-fold axis (Fig. 3). As a result of the fast electronic relaxation time of low spin Cr^{II} ($\tau_e \approx 10^{-12}$ s),[18] combined with minor delocalization of

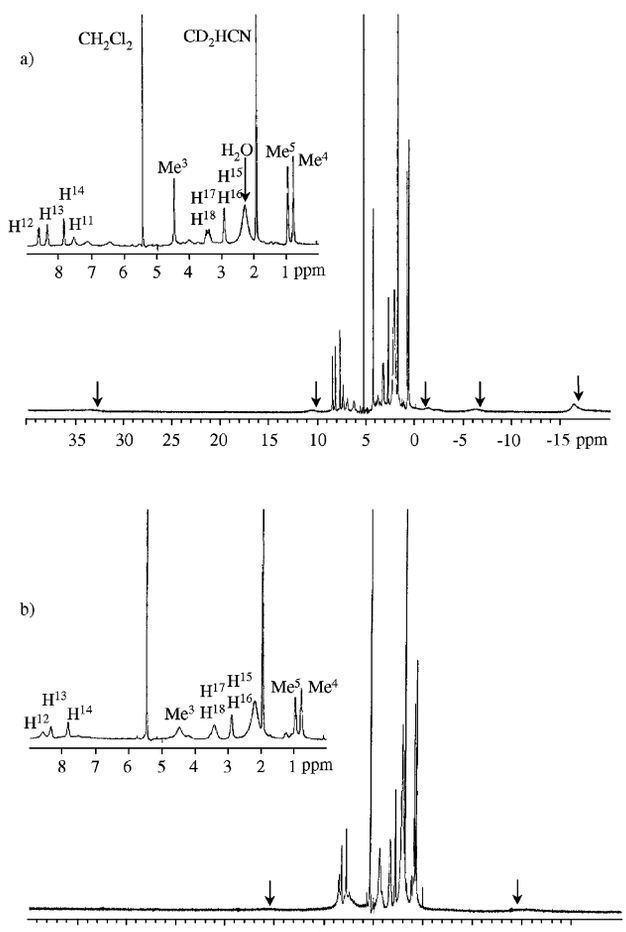

Fig. 3 ^{1}H NMR spectra (300 MHz) of a) (HHH)-$[LaCr^{II}L_3]^{5+}$ and b) (HHH)-$[LaCr^{III}L_3]^{6+}$ in CD_3CN (298 K, 3.8×10^{-2} mol dm^{-3}).

Table 1 Electronic spectral data for the heterodimetallic complexes (HHH)-$[LnCr^{II}L_3]^{5+}$ and (HHH)-$[LnCr^{III}L_3]^{6+}$ in acetonitrile at 293 K [a]

Compound	$\pi \longrightarrow \pi^*$	d–d + CT	Assignment [14]
L [b]	33250 (50700)		
	31750 (39100 sh)		
$[LaCr^{II}L_3]^{5+}$	40486 (83500)	23640 (6600 sh)	$^3T_1 \longrightarrow {}^3T_2$(b)
	30121 (93600)	20325 (3500)	$^3T_1 \longrightarrow {}^3E$(b)
		16475 (1700)	$^3T_1 \longrightarrow {}^3A_1 + {}^3A_2$
		14368 (2000 sh)	$^3T_1 \longrightarrow {}^3T_1 + {}^3T_2$(a)
		11710 (2700)	$^3T_1 \longrightarrow {}^3E$(a)
		9090 (2700 sh)	LMCT
		8368 (3800)	LMCT
$[EuCr^{II}L_3]^{5+}$	[c]	23640 (6300 sh)	$^3T_1 \longrightarrow {}^3T_2$(b)
	[c]	20408 (3000)	$^3T_1 \longrightarrow {}^3E$(b)
		16501 (1200)	$^3T_1 \longrightarrow {}^3A_1 + {}^3A_2$
		14368 (1500 sh)	$^3T_1 \longrightarrow {}^3T_1 + {}^3T_2$(a)
		11919 (2400)	$^3T_1 \longrightarrow {}^3E$(a)
		9090 (1900 sh)	LMCT
		8340 (2700)	LMCT
$[GdCr^{II}L_3]^{5+}$	[c]	23640 (5100 sh)	$^3T_1 \longrightarrow {}^3T_2$(b)
	[c]	20450 (2900)	$^3T_1 \longrightarrow {}^3E$(b)
		16475 (1800)	$^3T_1 \longrightarrow {}^3A_1 + {}^3A_2$
		14368 (1700)	$^3T_1 \longrightarrow {}^3T_1 + {}^3T_2$(a)
		11416 (1700)	$^3T_1 \longrightarrow {}^3E$(a)
		9090 (2800 sh)	LMCT
		8340 (4100)	LMCT
$[TbCr^{II}L_3]^{5+}$	[c]	23640 (7000 sh)	$^3T_1 \longrightarrow {}^3T_2$(b)
	[c]	20325 (3600)	$^3T_1 \longrightarrow {}^3E$(b)
		16475 (1800)	$^3T_1 \longrightarrow {}^3A_1 + {}^3A_2$
		14389 (2000 sh)	$^3T_1 \longrightarrow {}^3T_1 + {}^3T_2$(a)
		11723 (2700)	$^3T_1 \longrightarrow {}^3E$(a)
		9090 (2900 sh)	LMCT
		8306 (4200)	LMCT
$[LuCr^{II}L_3]^{5+}$	[c]	23640 (6500 sh)	$^3T_1 \longrightarrow {}^3T_2$(b)
	[c]	20408 (3500)	$^3T_1 \longrightarrow {}^3E$(b)
		16475 (1800)	$^3T_1 \longrightarrow {}^3A_1 + {}^3A_2$
		14389 (1900 sh)	$^3T_1 \longrightarrow {}^3T_1 + {}^3T_2$(a)
		11682 (2400)	$^3T_1 \longrightarrow {}^3E$(a)
		9090 (2900 sh)	LMCT
		8330 (4300)	LMCT
$[LaCr^{III}L_3]^{6+}$	40486 (78200 sh)	25700 (20600 sh)	
	30030 (102200)	22800 (2000 sh)	$^4A_2 \longrightarrow {}^4T_2 + {}^4T_1$
		21600 (1600 sh)	+CT
		20000 (700 sh)	
$[EuCr^{III}L_3]^{6+}$	40486 (99600 sh)	25700 (26000 sh)	
	29940 (126500)	22800 (2300 sh)	$^4A_2 \longrightarrow {}^4T_2 + {}^4T_1$
		21600 (1800 sh)	+CT
		20000 (700 sh)	
$[GdCr^{III}L_3]^{6+}$	40486 (100000 sh)	25700 (26000 sh)	$^4A_2 \longrightarrow {}^4T_2 + {}^4T_1$
	29940 (130000)	22800 (2400 sh)	+CT
		21600 (1900 sh)	
		20000 (800 sh)	
$[TbCr^{III}L_3]^{6+}$	40486 (79900 sh)	25700 (21000 sh)	
	29940 (103000)	22800 (2100 sh)	$^4A_2 \longrightarrow {}^4T_2 + {}^4T_1$
		21600 (1700 sh)	+CT
		20000 (700 sh)	
$[LuCr^{III}L_3]^{6+}$	40486 (74500 sh)	25700 (19500 sh)	
	29940 (95800)	22800 (1800 sh)	$^4A_2 \longrightarrow {}^4T_2 + {}^4T_1$
		21600 (1400 sh)	+CT
		20000 (600 sh)	

[a] Energies are given for the maximum of the band envelope in cm^{-1} and ε (in parentheses) in $M^{-1}\ cm^{-1}$; sh = shoulder, CT = charge transfer, LMCT = ligand-to-metal charge transfer. [b] Taken from ref. 16. [c] Saturation of the signal at the concentration investigated, dilution has been performed only for (HHH)-$[LaCr^{II}L_3]^{5+}$.

the unpaired electrons,[19] ^{1}H NMR signals are obtained for all protons of the coordinated ligands, but reliable assignment can only be obtained for the tridentate segment (by using 2D-COSY and NOESY techniques) because Cr^{II}-induced nuclear dipolar relaxation prevents scalar and dipolar couplings to be detected for the bidentate binding units connected to Cr^{II} (Fig. 3a).[18–20] The simultaneous consideration of absorption and NMR data implies that the C_3-symmetrical triple-helical non-covalent podates (HHH)-$[LnCr^{II}L_3]^{5+}$ are formed quantitatively in acetonitrile under stoichiometric conditions and for total ligand concentrations in the range 10^{-2}–10^{-3} mol dm^{-3}. It is remarkable that all studied lanthanides (including Eu^{III}) tolerate the introduction of the highly reducing Cr^{II} partner in the self-assembly process.

Post-assembly oxidation process leading to (HHH)-$[LnCr^{III}L_3]^{6+}$ (Ln = La, Eu, Gd, Tb, Tm, Lu)

Deep green solutions of (HHH)-$[LnCr^{II}L_3]^{5+}$ turn to pale orange within a few minutes upon diffusion of air. Low energy $L \longrightarrow Cr^{II}$ LMCT and spin-allowed Cr^{II}-centred d–d transitions occurring in the near-IR-visible domain are replaced by shoulders on the low-energy side of the ligand-centred $\pi \longrightarrow \pi^*$ transitions (Fig. 2). According to the original work of König and

Herzog dedicated to $[Cr(bipy)_3]^{3+}$,[14] the expected spin-allowed $^4A_2 \longrightarrow {}^4T_2$ and $^4A_2 \longrightarrow {}^4T_1$ transitions are mixed with low-lying MLCT transitions which prevents detailed assignments and reliable calculations of ligand field strength (Table 1).[14,21] However, a rough estimation of $10Dq$ can be obtained from the centre of gravity of the vibrational components of the $^4A_2 \longrightarrow {}^4T_2$ transition:[2,14] we get $10Dq \approx 21500$ cm^{-1} for Cr^{III} in (HHH)-$[LnCr^{III}L_3]^{6+}$ from the three components collected in Table 1, which can be compared with $10Dq = 23400$ cm^{-1} previously reported for $[Cr(bipy)_3]^{3+}$. As shown for the Cr^{II} complexes, 2,2′-bipyridine provides a slightly stronger ligand field than pyridylbenzimidazole because one six-membered ring is replaced by a five-membered ring in the bidentate segment of L.[15] The spin-forbidden $^4A_2 \longrightarrow {}^2E$, $^4A_2 \longrightarrow {}^2T_1$ and $^4A_2 \longrightarrow {}^2T_2$ transitions are too weak to be detected at millimolar concentrations in acetonitrile, but the Cr^{III}-centred $^2E \longrightarrow {}^4A_2$ transitions can be observed in the emission spectra (*vide infra*). Monitoring the oxidation process of (HHH)-$[LaCr^{II}L_3]^{5+}$ by ^{1}H NMR shows an extreme broadening for the protons of the bidentate segment connected to the slow-relaxing Cr^{III} ion (HHH)-$[LaCr^{III}L_3]^{6+}$ ($\tau_e \approx 10^{-9}$ s).[20] On the other hand, the protons belonging to the tridentate segment coordinated to diamagnetic La^{III} exhibit less dramatic broadening and only minor changes in chemical shifts when going from (HHH)-$[LnCr^{II}L_3]^{5+}$ to (HHH)-$[LnCr^{III}L_3]^{6+}$. The strict preservation of the number of signals observed for the tridentate units together with the absence of new splittings occurring upon oxidation point to the exclusive formation of the C_3-symmetrical complex (HHH)-$[LnCr^{III}L_3]^{6+}$. Finally, ESI–MS spectra of oxidized solutions (Ln = La, Eu, Gd, Tb, Tm, Lu) unambiguously confirm the formation of $[LnCr^{III}L_3]^{6+}$ which are characterized by their molecular peaks and their gas-phase adducts with triflate counter ions $[LnCr^{III}L_3(CF_3SO_3)_n]^{(6-n)+}$ (n = 1–4, Table S1, ESI).[22] Minor amounts of $[Cr^{III}L_3]^{3+}$ (and its adduct $[Cr^{III}L_3(CF_3SO_3)]^{2+}$) result from partial de-complexation of Ln^{III} occurring in the gas-phase and/or in solution, while traces of complexes with 1 : 2 stoichiometry $[LnCr^{III}L_2(CF_3SO_3)_n]^{(6-n)+}$ (n = 3, 4) suggest possible contamination of 1 : 3 complexes. Addition of $[(^nBu)_4N]CF_3SO_3$ in concentrated acetonitrile solutions of crude (HHH)-$[LnCr^{III}L_3]^{6+}$, followed by fractional crystallisation with diethyl ether provide orange crystals of $[LnCr^{III}L_3](CF_3SO_3)_6 \cdot mH_2O$ (Ln = La, m = 2: **1**; Ln = Eu, m = 4: **2**; Ln = Gd, m = 6: **3**; Ln = Tb, m = 3: **4**; Ln = Tm, m = 4: **5**; Ln = Lu, m = 2: **6**) in 33–68% yield after separation of a waxy brown precipitate. Elemental analyses support the proposed formulations (Table S2, ESI) and the IR spectra display the bands characteristic of the coordinated ligands ($\nu_{C=O}$ and $\nu_{C=N}$ in the 1600–1450 cm^{-1} range),[16] together with vibrations typical of ionic triflates.[23] X-Ray quality prisms have been obtained by slow diffusion of diethyl ether into concentrated acetonitrile solutions of **2** (Ln = Eu) and **6** (Ln = Lu).

Crystal and molecular structures of (HHH)-$[LnCrL_3](CF_3SO_3)_6(CH_3CN)_4$ (Ln = Eu, 7; Ln = Lu, 8)

The crystal structures of **7** and **8** consist of discrete cations (HHH)-$[LnCr^{III}L_3]^{6+}$ (Ln = Eu, **7**; Ln = Lu, **8**), six uncoordinated triflate anions and four solvent molecules. The two complexes are isostructural and the discussion is focused on **8**; comparisons with data obtained for **7** being presented when necessary. The atomic numbering scheme is presented in Fig. 4. Fig. 5 displays a view of the cation and Table 2 collects selected geometrical parameters.

The molecular structure of (HHH)-$[LuCr^{III}L_3]^{6+}$ is similar to that reported for (HHH)-$[LnCo^{III}L_3]^{6+}$ [11] in which a Co^{III} (six-coordinate ionic radius for low spin Co^{III}: $R_{CN=6}^{Co} = 0.545$ Å) is replaced by a slightly larger Cr^{III} ion ($R_{CN=6}^{Cr} = 0.615$ Å).[24] The chromium and lutetium metals define a pseudo-C_3 axis about which three ligand strands are helically wrapped in a head-to-head-to-head arrangement, to give the triple-helical cation

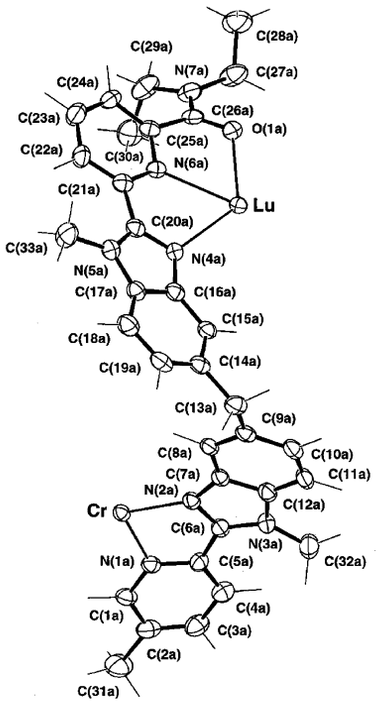

Fig. 4 Numbering scheme for the cation (HHH)-$[LuCr^{III}L_3]^{6+}$ in **8**. (Indices b and c correspond to the other strands). Ellipsoids are represented at the 40% probability level.

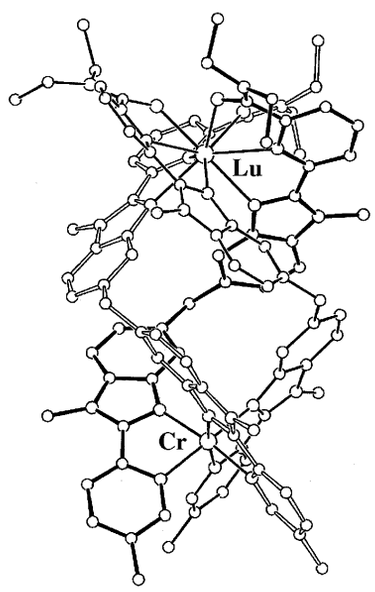

Fig. 5 Projection of (HHH)-$[LuCr^{III}L_3]^{6+}$ perpendicular to the pseudo-C_3 axis.

(HHH)-$[LuCr^{III}L_3]^{6+}$. The nine-coordinate lutetium atom occupies a pseudo-tricapped trigonal prismatic site in $[LuCr^{III}L_3]^{6+}$ with standard Lu–N(bzim) (2.502(4)–2.518(4) Å, average 2.51(1) Å), Lu–N(py) (2.514(4)–2.551(4) Å, average 2.53(1) Å) and Lu–O(amide) (2.317(3)–2.349(4) Å, average 2.32(2) Å) bond distances which are similar to those observed for $[LuCo^{III}L_3]^{6+}$.[11] The classical geometrical analysis of the lanthanide site based on a trigonally distorted pseudo-tricapped trigonal prismatic geometry[11] shows no major difference between $[LuCr^{III}L_3]^{6+}$ and $[LuCo^{III}L_3]^{6+}$ (ϕ, θ_i and ω_i angles are given in Table S5 in the ESI).

The Cr^{III} coordination sphere in $[LuCr^{III}L_3]^{6+}$ is best described as a distorted octahedron flattened along the molecular pseudo-C_3 axis. The Cr–N bond distances are longer than the related Co–N distances reported for $[LuCo^{III}L_3]^{6+}$ in agreement with the change in the respective ionic radii of the central

Table 2 Selected bond distances (Å) and angles (°) for $[LnCrL_3](CF_3SO_3)_6(CH_3CN)_4$ (Ln = Eu, **7**; Ln = Lu, **8**)

	Ligand a		Ligand b		Ligand c	
	8	**7**	**8**	**7**	**8**	**7**
Ln ··· Cr	9.3546(9)	9.3238(8)				
Ln–O(1)	2.349(4)	2.422(4)	2.302(3)	2.397(3)	2.317(3)	2.383(3)
Ln–N(4)	2.518(4)	2.592(4)	2.502(4)	2.575(4)	2.509(4)	2.573(4)
Ln–N(6)	2.514(4)	2.599(4)	2.515(4)	2.602(4)	2.551(4)	2.624(4)
Cr–N(1)	2.071(4)	2.073(4)	2.070(4)	2.079(4)	2.078(4)	2.087(4)
Cr–N(2)	2.019(4)	2.018(4)	2.020(4)	2.027(4)	2.022(4)	2.025(4)

	Ligand a		Ligand b		Ligand c	
Bite angles	**8**	**7**	**8**	**7**	**8**	**7**
N(1)–Cr–N(2)	79.5(1)	79.6(2)	79.4(1)	79.6(1)	79.0(2)	79.4(2)
N(4)–Ln–N(6)	64.0(1)	62.1(1)	64.6(1)	62.6(1)	64.3(1)	63.0(1)
N(6)–Ln–O(1)	64.6(1)	63.4(1)	64.8(1)	63.7(1)	64.7(1)	63.2(1)
N(4)–Ln–O(1)	128.5(1)	125.3(1)	129.3(1)	126.3(1)	129.0(1)	126.1(1)

N–Cr–N						
	8	**7**			**8**	**7**
N(1a)–Cr–N(2b)	89.3(2)	89.0(2)		N(1a)–Cr–N(1c)	95.5(2)	95.5(2)
N(1a)–Cr–N(2c)	174.0(2)	174.4(2)		N(2a)–Cr–N(1b)	171.4(2)	171.3(2)
N(2a)–Cr–N(2b)	97.6(1)	97.4(2)		N(2a)–Cr–N(1c)	87.7(2)	87.7(2)
N(2a)–Cr–N(2c)	97.7(1)	97.8(2)		N(1a)–Cr–N(1b)	92.3(2)	92.1(2)
N(1b)–Cr–N(1c)	95.8(2)	95.9(2)		N(1b)–Cr–N(2c)	90.7(2)	90.8(2)
N(2b)–Cr–N(1c)	173.4(2)	173.7(2)		N(2b)–Cr–N(2c)	96.4(2)	96.3(2)

N–Ln–N						
	8	**7**			**8**	**7**
N(4a)–Ln–N(4b)	85.0(1)	86.1(1)		N(6a)–Ln–N(6b)	121.5(1)	121.7(1)
N(4b)–Ln–N(4c)	84.9(1)	85.8(1)		N(6b)–Ln–N(6c)	119.2(1)	118.7(1)
N(4a)–Ln–N(4c)	87.4(1)	88.7(1)		N(6a)–Ln–N(6c)	118.2(1)	118.6(1)
N(4a)–Ln–N(6c)	146.9(1)	147.6(1)		N(4a)–Ln–N(6b)	74.5(1)	75.2(1)
N(6a)–Ln–N(4b)	142.1(1)	142.0(1)		N(4b)–Ln–N(6c)	76.1(1)	76.9(1)
N(6b)–Ln–N(4c)	145.4(1)	145.0(1)		N(6a)–Ln–N(4c)	73.0(1)	73.8(1)

O–Ln–N						
	8	**7**			**8**	**7**
N(4a)–Ln–O(1c)	140.7(1)	142.6(1)		N(4a)–Ln–O(1b)	80.0(1)	78.4(1)
N(6a)–Ln–O(1b)	68.7(1)	70.1(1)		N(6a)–Ln–O(1c)	133.6(1)	134.2(1)
N(6b)–Ln–O(1c)	66.7(1)	68.2(1)		N(4b)–Ln–O(1c)	84.2(1)	83.8(1)
O(1a)–Ln–N(6b)	132.9(1)	134.1(1)		O(1a)–Ln–N(4b)	142.7(1)	145.0(1)
O(1a)–Ln–N(4c)	81.3(1)	80.5(1)		O(1a)–Ln–N(6c)	66.6(1)	68.1(1)
O(1b)–Ln–N(4c)	141.5(1)	143.6(1)		O(1b)–Ln–N(6c)	132.9(1)	133.8(1)

O–Ln–O						
	8	**7**			**8**	**7**
O(1a)–Ln–O(1b)	78.6(1)	79.8(1)		O(1b)–Ln–O(1c)	78.1(1)	79.0(1)
O(1a)–Ln–O(1c)	78.0(1)	78.8(1)				

ion, but the increases of the M–N bond distances observed when going from Co–N(bzim) to Co–N(py) is maintained for M = Cr (average Cr–N(bzim) = 2.020(4) Å, average Cr–N(py) = 2.073(5) Å). Comparison with Cr–N(py) bonds in $[Cr(bipy)_3]^{3+}$ (2.042 Å)[25] points to minor mechanical constraints induced by (i) the lanthanide site onto the Cr^{III} coordination sphere and (ii) the replacement of a pyridine ring by a benzimidazole ring in the bidentate segment of the ligand L. The detailed geometrical analysis of the octahedral coordination site based on the angles ϕ, θ_i and ω_i (Fig. 6)[26] allows the quantitative estimation of fine structural distortions occurring around M^{III} in $[LuCr^{III}L_3]^{6+}$, $[Cr(bipy)_3]^{3+}$ and $[LuCo^{III}L_3]^{6+}$ (Table 3 and Tables S6 and S7, ESI).

For the three complexes, we observe no significant deviation from the pseudo-axial C_3 symmetry as measured by ϕ = 178–180° which lies close to the ideal value of 180° for a perfect octahedron. The flattening along the pseudo-C_3 axis is significant (θ_i = 57–61° compared to 54.7° for a perfect octahedron) and can be traced back to the structural restriction imposed by the fixed bite angles of semi-rigid chelating bipyridine or pyridylbenzimidazole binding units.[26] However, similar θ_i values are calculated for Co^{III} and Cr^{III} coordination spheres pointing to comparable arrangements of the donor atoms around M^{III} in both non-covalent podates. The only significant difference

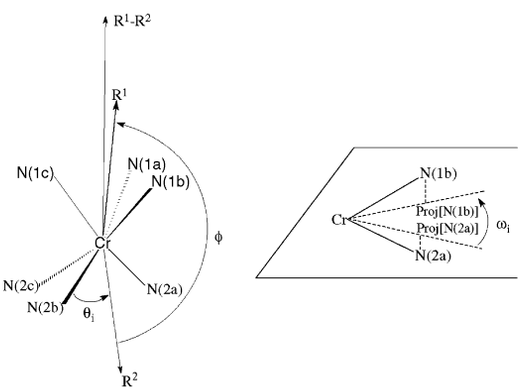

Fig. 6 Definition of ϕ, θ_i and ω_i for a pseudo-octahedral site (R^1 = Co–N(1a) + Co–N(1b) + Co–N(1c) and R^2 = Co–N(2a) + Co–N(2b) + Co–N(2c)).[26] Proj[N(*i*)] is the projection of N(*i*) along the R^1–R^2 direction onto a perpendicular plane passing through the metal.

arises from the wrapping of the bidentate ligand strands about the metal ion measured by the ω_i angles. For $[Cr(bipy)_3]^{3+}$, ω_i = 49° significantly deviates from the octahedron (ω_i = 60°) toward a trigonal prism (ω_i = 0°). In $[LuCr^{III}L_3]^{6+}$, the connection to the second metallic site and/or the replacement of a pyridine ring

Table 3 Selected structural data[a] for the chromium coordination sphere in $[LuCrL_3](CF_3SO_3)_6(CH_3CN)_4$ (**8**), $[Cr(bipy)_3](PF_6)_3$[25] and for the cobalt coordination sphere in $[LuCoL_3](CF_3SO_3)_6(CH_3CN)_2(H_2O)$[11]

	Angles[a] ϕ/°		
	(HHH)-$[LuCrL_3]^{6+}$	$[Cr(bipy)_3]^{3+}$	(HHH)-$[LuCoL_3]^{6+}$
R^1–M–R^2	179	180	178
	Angles θ_i/° (distal tripods)[a]		
R^1–M–N(1a)	57	58	59
R^1–M–N(1b)	57	58	58
R^1–M–N(1c)	60	58	58
R^2–M–N(2a)	61	58	59
R^2–M–N(2b)	60	58	60
R^2–M–N(2c)	60	58	57
	Angles ω_i/° (intraligand)[a]		
Proj[N(1a)]–M–Proj[N(2a)][b]	53	49	57
Proj[N(1b)]–M–Proj[N(2b)]	51	49	56
Proj[N(1c)]–M–Proj[N(2c)]	53	49	56

[a] For the definition of ϕ, θ_i and ω_i, see Fig. 6.[26] The error in the angles is a maximum of 1°. [b] Proj[N(i)] is the projection of N(i) along the R^1–R^2 direction onto a perpendicular plane passing through the metal. R^1 = M–N(1a) + M–N(1b) + M–N(1c) and R^2 = M–N(2a) + M–N(2b) + M–N(2c).

with a benzimidazole unit slightly reduces this distortion (average ω_i = 52°), a trend which is even more pronounced for $[LuCo^{III}L_3]^{6+}$ (average ω_i = 56°). We conclude that the ligands are less tightly wrapped around Cr^{III} (compared to Co^{III}), a structural variation which is expected to increase the intermetallic Lu ··· Cr distance because of mechanical coupling and the spring effect in dimetallic helicates.[11] A detailed analysis of each helical portion delimited by the five almost parallel (interplanar angles 1–16° for $[LuCr^{III}L_3]^{6+}$ and 1–18° for $[LuCo^{III}L_3]^{6+}$, Table S3, ESI) facial planes F_1–F_5 (F_1: N1a, N1b, N1c; F_2: N2a, N2b, N2c; F_3: N4a, N4b, N4c; F_4: N6a, N6b, N6c; F_5: O1a, O1b, O1c, Scheme 1) packed along the pseudo-C_3

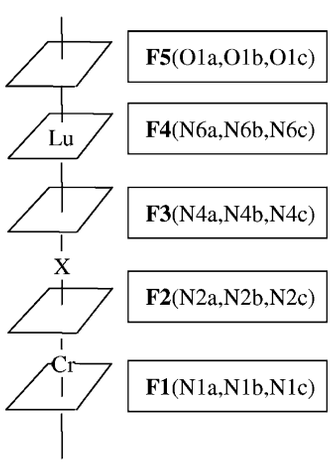

Scheme 1

axis[11] shows similar helical behaviours for $[LuM^{III}L_3]^{6+}$ (M = Cr, Co; Table S8, ESI)[28] except for the F_1–F_2 portion where the wrapping of the strands is considerably relaxed around Cr^{III}. We can thus safely ascribe the larger Lu ··· Cr distance in $[LuCr^{III}L_3]^{6+}$ (9.3546(9) Å in **8** compared to 9.234(2) Å found in $[LuCo^{III}L_3]^{6+}$)[11] to the minor structural variations detected in the coordination spheres of the d-block ions.[27]

The triple-helical cations $[LuCr^{III}L_3]^{6+}$ are oriented in the crystal with their pseudo-C_3 axis roughly aligned with the *a* direction (5.7°) and packed into columns in a pseudo-hexagonal arrangement. Within each column, the Ln–Cr orientations and the screw sense are identical and the intermolecular Ln ··· Cr distance between two packed helices amounts to 13.018(1) Å. The triflate anions and solvent molecules occupy the interstices between the columns (Fig. S1, ESI).

Since the crystal structures of $[EuCrL_3](CF_3SO_3)_6(CH_3CN)_4$ (**7**) is isostructural with **8**, identical packing of the triple helices, anions and solvent molecules is observed in the crystals. The molecular structures of the cations $[LnCr^{III}L_3]^{6+}$ (Ln = Eu, **7**, Ln = Lu, **8**) are almost identical (Fig. S2, ESI) except for the expected expansion of the lanthanide coordination sphere in going from Lu to Eu. However, the 0.07–0.08 Å increase in the Eu–N and Eu–O bond distances (Table 2) is smaller than the difference between the ionic radii of the nine-coordinate metal ions: $\Delta R = R^{Eu}_{CN=9} - R^{Lu}_{CN=9}$ = 1.120–1.032 = 0.088 Å.[24] Calculation of ionic radii for Ln^{III} ions in $[LnCr^{III}L_3]^{6+}$ (Ln = Eu, **7**, Ln = Lu, **8**) according to Shannon's definition with r(N) = 1.46 Å and r(O) = 1.31 Å gives R^{Eu} = 1.120 Å and R^{Lu} = 1.043 Å and points to a standard arrangement around Eu^{III}, but to an unusual expansion around Lu^{III} ($R^{Lu}_{CN=9}$ = 1.032 Å).[24] Finally the Eu ··· Cr distance (9.3238(8) Å) only marginally deviates from that found for **8** in agreement with a rather rigid organisation of the ligand strands in the final complexes.

Photophysical properties of $[LnCr^{III}L_3](CF_3SO_3)_6\cdot mH_2O$ (Ln = La, *m* = 2: 1; Ln = Eu, *m* = 4: 2; Ln = Gd, *m* = 6: 3; Ln = Tb, *m* = 3: 4; Ln = Tm, *m* = 4: 5; Ln = Lu, *m* = 2: 6)

The reflectance spectra of complexes **2**–**4** in the solid state display strong π ⟶ π* transitions centred at 28570 cm^{-1} together with a broad and weaker band at 20000 cm^{-1} assigned to the first spin-allowed Cr^{III}-centred $^4A_2 \longrightarrow {}^4T_2$ transition in agreement with related transitions observed for $[LnCr^{III}L_3]^{6+}$ (Ln = La, Eu, Gd, Tb, Lu) in solution (Table 1). Interestingly, the Eu-complex **2** exhibits a broad shoulder around 25000 cm^{-1} which is absent in the Gd (**3**) and Tb (**4**) analogues and consecutively ascribed to the L ⟶ Eu^{III} LMCT transition expected in this spectral range.[16,29] Considering the Racah parameter B = 730 cm^{-1} found for $[Cr(bipy)_3]^{3+}$ [14,25] and $10Dq \approx$ 21500 cm^{-1} for Cr^{III} in (HHH)-$[LnCr^{III}L_3]^{6+}$, we calculate $10Dq/B \approx 29$ and predict from the Tanabe–Sugano diagrams for the d^3 configuration, that the next spin-allowed Cr^{III}-centred $^4A_2 \longrightarrow {}^4T_1$ transition lies around 27500 cm^{-1}, a spectral range masked by intense ligand-centred π ⟶ π* transitions. According to this rough calculation, the lowest Cr^{III}-centred excited state ^2E is expected at 13340 cm^{-1} (Fig. 7).

Cr^{III}-centred luminescence in $[GdCrL_3](CF_3SO_3)_6\cdot 6H_2O$ (3)

Excitation through the ligand-centred $^1\pi\pi^*$ (29400 cm^{-1}, S_1 level in Fig. 7) or Cr^{III}-centred $^4A_2 \longrightarrow {}^4T_2$ (20492 cm^{-1}) levels of **3** at 10 K provides identical emission spectra showing exclusively the characteristic $^2E \longrightarrow {}^4A_2$ transition (13301 cm^{-1}) combined with weak Stokes phonon sidebands (12997–12840 cm^{-1}, Fig. 7 and Fig. S3, ESI).[25] Since (i) Gd^{III} does not possess

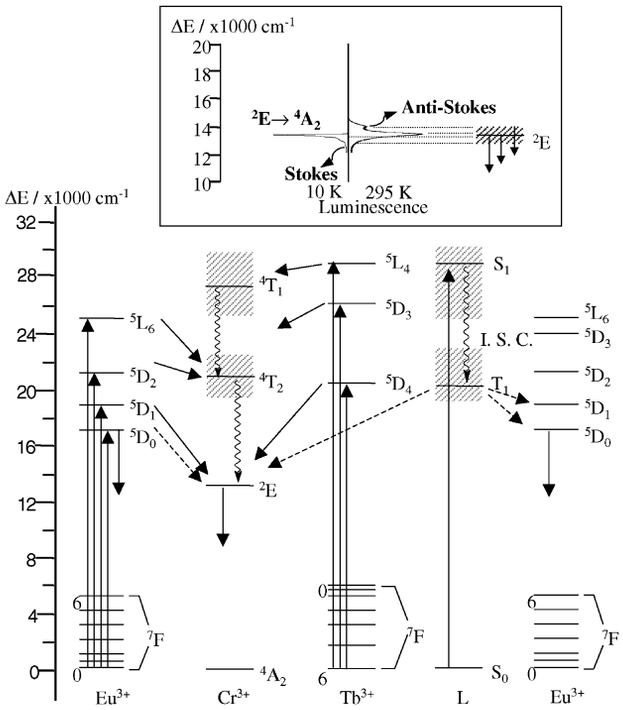

Fig. 7 Partial energy level diagram showing ground and excited levels centred on the metals (Cr^{III}, Eu^{III}, Tb^{III}) and ligand L, and summarizing the excitation processes, energy transfers and radiative emission processes investigated in this study for (HHH)-$[LnCrL_3](CF_3SO_3)_6$ (Ln = Eu, **2** and Ln = Tb, **4**). The $Cr(^2T_1, {}^2T_2)$ levels are omitted for clarity although they can act as a relay for energy transfer processes (see text).

accessible excited states below 32200 cm^{-1} [30] and (ii) no residual emission originating from the ligand-centred $^1\pi\pi^*$ or $^3\pi\pi^*$ (T_1 level in Fig. 7) states is detected (zero-phonon transitions are expected respectively at 26300 cm^{-1} ($^1\pi\pi^*$) and 19960 cm^{-1} ($^3\pi\pi^*$) according to the emission spectrum of $[GdZnL_3]^{5+}$),[16] we conclude that efficient L ⟶ Cr^{III} energy transfer processes channel the electronic energy toward the lowest emitting ^2E state. The characteristic $Cr(^2E)$ lifetime does not depend on the excitation wavelength and it is rather long (3.3–3.6 ms at 10 K, Table 4) pointing to only minor non-radiative processes affecting the Cr^{III}-centred emission in $[GdCrL_3]^{6+}$ at 10 K. However, the intensity of the $Cr(^2E)$ emission dramatically decreases with increasing temperature (Fig. S5, ESI) and the associated lifetime observed at 295 K (0.2–0.3 ms) involves the existence of thermally-activated non-radiative vibrational quenching processes combined with energy migration processes as previously reported for Cr^{III}-containing coordination networks in which a temperature of 1.5 K is required to 'freeze' such processes.[31] As the maximum of the emission band shifts from 13301 cm^{-1} at 10 K to 13347 cm^{-1} at 295 K (Fig. S3, ESI), we suspect that the long-lived luminescence observed at low temperature and originating from isolated pseudo-octahedral CrN_6 chromophores in $[GdCrL_3]^{6+}$ is mainly quenched at room temperature leading to a faint residual emission arising from crystal defects or 'killer sites' produced by minor photochemical degradation.[7] Finally, the excitation spectrum of **3** at 10 K recorded upon monitoring the $^2E \longrightarrow {}^4A_2$ transition shows a broad band covering the 19450–22270 cm^{-1} spectral range and assigned to the $^4A_2 \longrightarrow {}^4T_2$ transition (mixed with CT transitions) previously observed in the absorption spectra (Table 1). Unfortunately, the 2nd order Rayleigh band prevents detection of the excitation profile arising from the ligand-centred $^1\pi\pi^*$ state.

Eu^{III}-centred luminescence in $[EuCrL_3](CF_3SO_3)_6\cdot 4H_2O$ (2) and $[EuCrL_3](CF_3SO_3)_6(CH_3CN)_4$ (7)

Upon excitation through the ligand-centred $^1\pi\pi^*$ state at 28329 cm^{-1} or selective laser excitation of the Eu-centred

Table 4 Lifetimes of the $Eu(^5D_0)$ and $Cr(^2E)$ excited levels (ms) in $[LnCr^{III}L_3](CF_3SO_3)_6\cdot mH_2O$ and $[EuCr^{III}L_3](CF_3SO_3)_6(CH_3CN)_4$ (**7**) in the solid-state under various excitation conditions (analysing wavelength sets on the maximum of the $^5D_0 \longrightarrow {}^7F_2$ or $^2E \longrightarrow {}^4A_2$ transition)

T/K	Compound	λ_{ex}/cm^{-1}	λ_{an}/cm^{-1}	τ/ms
10	$[GdCrL_3]^{6+}$ (**3**)	28329	13301	3.66(3) $Cr(^2E)$
		21322	13301	3.62(1) $Cr(^2E)$
		17216	13301	3.30(2) $Cr(^2E)$
295		28329	13348	0.29(1) $Cr(^2E)$
		21322	13348	0.19(1) $Cr(^2E)$
		17216	13348	0.33(1) $Cr(^2E)$
10	$[EuCrL_3]^{6+}$ (**2**)	28329	13301	3.46(1) $Cr(^2E)$
		17216	13305	3.36(3) $Cr(^2E)$
295		28329	13348	0.09(1) $Cr(^2E)$
		17224	13348	0.15(1) $Cr(^2E)$
10		28329	16218	0.55(4) $Eu(^5D_0)$
		17216	16218	0.59(1) $Eu(^5D_0)$
295		28329	16218	0.59(1) $Eu(^5D_0)$
		17224	16218	0.62(1) $Eu(^5D_0)$
295[a]	$[EuCrL_3]^{6+}$ (**2**)[a]	28329	16218	0.87(4) $Eu(^5D_0)$
10	$[EuCrL_3]^{6+}$ (**7**)	28329	13200	3.12(1) $Cr(^2E)$
		17216	13193	3.03(1) $Cr(^2E)$
295		28329	13348	0.05(1) $Cr(^2E)$
		17224	13348	0.05(1) $Cr(^2E)$
10		28329	16218	0.75(1) $Eu(^5D_0)$
		17216	16218	0.76(1) $Eu(^5D_0)$
295		28329	16218	0.66(1) $Eu(^5D_0)$
		17224	16218	0.66(1) $Eu(^5D_0)$
10	$[TbCrL_3]^{6+}$ (**4**)	28329	13300	3.39(1) $Cr(^2E)$
		20492	13300	3.42(1) $Cr(^2E)$
		21286	13300	3.35(1) $Cr(^2E)$
295		28329	13348	—
		20492	13348	0.17(1) $Cr(^2E)$
		21249	13348	0.17(1) $Cr(^2E)$

[a] 10^{-4} mol dm^{-3} in acetonitrile.

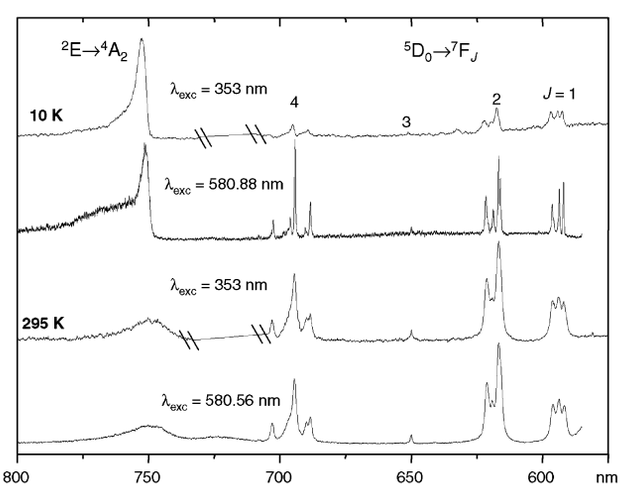

Fig. 8 Emission spectra of (HHH)-$[EuCrL_3](CF_3SO_3)_6\cdot 4H_2O$ (**2**) in the solid state at 10 and 295 K (‖—‖: Rayleigh band suppressed).

$^5D_0 \longleftarrow {}^7F_0$ transition (17216 cm^{-1}) of **2** at 10 K, the emission spectra display narrow bands corresponding to Eu-centred $^5D_0 \longrightarrow {}^7F_J$ transitions (J = 0–4, 17216–14233 cm^{-1}) along with the Cr-centred $^2E \longrightarrow {}^4A_2$ transition at 13301 cm^{-1} (Fig. 8). The detection of only a faint residual ligand-centred $^1\pi\pi^*$ emission around 20000–25000 cm^{-1} points to quasi-quantitative L ⟶ Cr^{III} and/or L ⟶ Eu^{III} energy transfer processes in these complexes. The integrated emission intensity upon excitation of the ligand-centred $^1\pi\pi^*$ states shows that $Cr(^2E \longrightarrow {}^4A_2)$ corresponds to 73% of the total emission of the complex, the remaining 27% arising from $Eu(^5D_0 \longrightarrow {}^7F_J)$ transitions (Table S9, ESI). This ratio changes to 51/49 upon selective irradiation of the $Eu(^5D_0)$ level, while increasing the temperature drastically reduces the contribution of the Cr-emission as expected from

Table 5 Identified Eu(^7F_J) crystal field levels (cm^{-1}, J = 1–4) in $[EuCrL_3](CF_3SO_3)_6\cdot 4H_2O$ (**2**) as determined from luminescence spectra at 10 and 295 K (excitation through the $^5D_0$ level taken as the origin)

10 K					295 K				
$^5D_0$	$^7F_1$	$^7F_2$	$^7F_3$	$^7F_4$	$^5D_0$	$^7F_1$	$^7F_2$	$^7F_3$	$^7F_4$
17216	320	980	1829	2697	17224	320	987	1839	2696
	368	997		2724		377	1007		2727
	444	1053		2806		445	1069		2822
		1113		2846			1106		2870
		1127		2894			1122		2995
				2983					

the existence of thermally-activated energy migration and quenching processes previously discussed for $[GdCrL_3]^{6+}$. Selective excitation of Eu-centred levels of higher energy ($^5L_6 \leftarrow {}^7F_0$ at 25316 cm^{-1}, $^5D_2 \leftarrow {}^7F_0$ at 21459 cm^{-1} and $^5D_1 \leftarrow {}^7F_0$ at 18975 cm^{-1}) yields exclusively Cr-centred emission which implies quantitative Eu ⟶ Cr energy transfers resulting from efficient resonances between these narrow Eu-centred levels and the broad Cr-centred $^4T_2$ and $^4T_1$ levels.[9,32,33] The lowest Eu-centred $^5D_0$ level (17216 cm^{-1}) escapes complete quenching *via* energy transfer to Cr^{III} because of the poor energy match with the acceptor $Cr(^2E)$ and $Cr(^2T_1)$ levels (Fig. 7). Parallel studies with single crystals of **7** display similar trends at 10 K, but the Eu-centred emission dominates spectra at room temperature (94–99% of the total intensity) in agreement with our hypothesis that crystal defects are responsible for the observation of residual Cr-centred luminescence at room temperature. We indeed expect that the probability of crystal defects is larger for **2** because the removal of acetonitrile molecules from **7** and their replacement by water molecules in **2** destroy the single crystals and produce amorphous materials.

The high-resolution excitation profile of the $^5D_0 \leftarrow {}^7F_0$ transition in $[EuCrL_3]^{6+}$ (**2**) displays a single sharp and symmetrical peak at 17216 cm^{-1} at 10 K (full width at half height fwhh = 4.2 cm^{-1}) which is shifted to 17224 cm^{-1} at 295 K (fwhh = 6.9 cm^{-1}). This value is typical of a Eu^{III} ion nine-coordinated by six heterocyclic nitrogen atoms and three carboxamide oxygen donors (the empirical equation of Frey and Horrocks suggests 17223 cm^{-1} at 295 K)[16,34] and it can be compared with 17220 cm^{-1} found for $[EuZnL_3]^{5+}$ at 10 K.[16] Detailed analysis of the crystal field splitting (Table 5) is consistent with a distorted trigonal micro-symmetry around Eu^{III}. The extremely weak $^5D_0 \longrightarrow {}^7F_0$ emission agrees with its assignment to a symmetry-forbidden transition in the D_3 point group, but the peculiar splitting of the $^5D_0 \longrightarrow {}^7F_1$ transition (two main transitions $A_1 \longrightarrow A_2$ and $A_1 \longrightarrow E$ separated by 100 cm^{-1}, the latter being further split by 48 cm^{-1}) indicates a significant deviation from trigonal symmetry as previously discussed for $[EuZnL_3]^{5+}$ ($A_1 \longrightarrow A_2$ and $A_1 \longrightarrow E$ separated by 128 cm^{-1}, the latter being further split by 21 cm^{-1}).[16] The analysis of the $^5D_0 \longrightarrow {}^7F_2$ transition shows two intense doublets ($2\times A_1 \longrightarrow E$ in D_3 further split by 14 and 17 cm^{-1} respectively (Table 5)) and one weaker singlet ($A_1 \longrightarrow A_1$ forbidden in D_3) which is coherent with a distorted trigonal symmetry and the observation of four intense and two weak components for the $^5D_0 \longrightarrow {}^7F_4$ transition (six transitions expected in D_3 symmetry: $A_1 \longrightarrow A_2$ and $3\times A_1 \longrightarrow E$ are magnetic and dipole allowed and $2\times A_1 \longrightarrow A_1$ are forbidden).[35] We conclude that the crystal field around Eu^{III} in $[EuCrL_3]^{6+}$ and in $[EuZnL_3]^{5+}$ [16] are similar and derive from pseudo-trigonal arrangements of the nine donor atoms.

Intermetallic energy transfers in $[EuCrL_3](CF_3SO_3)_6\cdot 4H_2O$ (2), $[EuCrL_3](CF_3SO_3)_6(CH_3CN)_4$ (7) and $[TbCrL_3](CF_3SO_3)_6\cdot 3H_2O$ (4)

The $Eu(^5D_0)$ lifetime in single crystals (**7**) does not depend on the excitation mode, through ligand-centred $^1\pi\pi^*$ or Eu-centred $^5D_0$ levels, but it is short (0.75(1) ms at 10 K and 0.66(1) ms at 295 K (Table 4)) compared to that reported for the analogous anhydrous $[EuZnL_3](ClO_4)(CF_3SO_3)_4(CH_3CN)_4$ complex: 2.53(1) ms at 10 K.[16] Since (i) no water molecule lies in the first coordination sphere of Eu^{III} in the crystal structure of **7**, and (ii) the interaction with interstitial water molecules in the second sphere produces comparable effects for **2** and $[EuZnL_3](ClO_4)_5(H_2O)_2$ (τ_{Eu} is reduced to 0.59(1) ms in **2** and to 2.19(1) ms in $[EuZnL_3](ClO_4)_5(H_2O)_2$),[16] the decrease of the Eu-centred lifetime observed in going from $[EuZnL_3]^{5+}$ to $[EuCrL_3]^{6+}$ at 10 K can be safely assigned to a Eu ⟶ Cr energy transfer process. The yield of the latter is given by $\eta = 1 - (\tau/\tau_0)$ in which τ and τ_0 are respectively the lifetime in the presence (observed for $[EuCrL_3]^{6+}$) and absence (observed for $[EuZnL_3]^{5+}$) of Cr^{III} quencher. We calculate η = 70(4)% for the anhydrous crystals and η = 73(4)% for the complexes containing interstitial water molecules at 10 K. Modelling the Eu ⟶ Cr energy transfer with a pure dipole–dipole mechanism (eqn. (1)) is reasonable accord-

$$\eta = 1 - \frac{\tau}{\tau_0} = \left[1 + \left(\frac{R}{R_0}\right)^6\right]^{-1} \quad (1)$$

ing to the large Eu ··· Cr distance measured in the crystal of **7** (R = 9.32 Å) and the minute expansion of the 4f orbitals.[33,35,36] The critical distance for 50% energy transfer amounts to $R_0 \approx$ 10.8 Å for the Eu/Cr pair in complexes **2** or **7** at 10 K. Identical calculations using lifetimes obtained at 295 K (0.59(1) ms for **2** and 1.67(2) ms for $[EuZnL_3](ClO_4)_5(H_2O)_2$ [16] give η = 65(3)% and $R_0 \approx$ 10.3 Å, thus pointing to a negligible effect of the temperature on the Eu ⟶ Cr energy transfer process.

In order to investigate the relative importance of intramolecular *versus* intermolecular Eu ⟶ Cr energy transfers on the quenching of the $Eu(^5D_0)$ level, we have recorded the emission spectrum for a 10^{-4} mol dm^{-3} acetonitrile solution of $[EuCrL_3](CF_3SO_3)_6\cdot 4H_2O$ in which negligible de-complexation is expected[16] and static intermolecular intermetallic energy transfers are removed. Upon irradiation at 29170 cm^{-1} (*via* the ligand-centred $^1\pi\pi^*$ state) at 295 K, we exclusively detect significant luminescence from the Eu-centred $^5D_0 \longrightarrow {}^7F_J$ (J = 1–6) transitions. As the weak $Eu(^5D_0 \longrightarrow {}^7F_5)$ component may overlap with $Cr(^2E \longrightarrow {}^4A_2)$ around 13300 cm^{-1}, we have recorded the emission spectra of $[GdCrL_3](CF_3SO_3)_6\cdot 6H_2O$ (**3**) under the same experimental conditions which displays faint to negligible emission in this spectral range in agreement with efficient non-radiative processes de-activating $Cr(^2E)$ at 295 K (freezing the solution at 10 K restores the $Cr(^2E \longrightarrow {}^4A_2)$ emission at 13358 cm^{-1}, τ = 4.48(5) ms). The high-resolution emission spectrum of $[EuCrL_3]^{6+}$ in acetonitrile closely matches that found in the solid state except for the expected broadening of the signals and we conclude that the triple-helical structure is maintained in solution as suggested from NMR data. The absolute quantum yield of $[EuCrL_3]^{6+}$ is low Φ_{EuCr} = 0.13(2)% (10^{-4} mol dm^{-3} in acetonitrile at 295 K) and can be compared to Φ_{EuZn} = 0.34(4)% for $[EuZnL_3]^{5+}$ measured under the same experimental conditions.[16] If we consider that the intramolecular Eu ⟶ Cr transfer in $[EuCrL_3]^{6+}$ is the only additional non-radiative process which affects the $Eu(^5D_0)$ level when Cr^{III}

replaces Zn^{II} in the pseudo-octahedral site, the efficiency of this energy transfer is given by $\eta = 1 - \Phi_{EuCr}/\Phi_{EuZn} = 0.62(17)$, a value close to $\eta = 0.65$–0.73 found for $[EuCrL_3]^{6+}$ in the solid state. Lifetime measurements confirm this trend and we calculate $\eta = 1 - (\tau/\tau_0) = 0.70(4)$ in solution with $\tau = 0.87(4)$ ms for $[EuCrL_3]^{6+}$ (Table 4) and $\tau_0 = 2.88(1)$ ms for $[EuZnL_3]^{5+}$ measured in solution in the same conditions[16] (the observation of slightly longer $Eu(^5D_0)$ lifetimes in solution is typical for heterodimetallic d–f helicates).[16,17,37] Although we cannot completely rule out some contributions of bimolecular dynamic quenching processes involving intermolecular energy transfers affecting $Eu(^5D_0)$ lifetimes in solution,[38] the identical rate of quenching of the $Eu(^5D_0)$ level ($\eta \approx 70\%$) observed in the solid state and in solution when a Zn^{II} partner in $[EuZnL_3]^{5+}$ is replaced by Cr^{III} in $[EuCrL_3]^{6+}$ strongly supports the existence of an efficient *intramolecular directional* Eu ⟶ Cr energy transfer occurring in **2** and **7**.

For $[TbCrL_3](CF_3SO_3)_6\cdot 3H_2O$ at 10 K, excitation through the ligand-centred $^1\pi\pi^*$ levels or selective excitation of the Tb-centred levels $^5L_4$ (27027 cm^{-1}), $^5D_3$ (26468 cm^{-1}) or $^5D_4$ (20492 cm^{-1}) produce emission spectra exhibiting exclusively the Cr-centred $^2E \longrightarrow {}^4A_2$ transition. The observation of weak Stokes phonon sidebands together with a dramatic reduction of the luminescence with increasing temperature exactly matches the spectra obtained for $[GdCrL_3](CF_3SO_3)_6\cdot 6H_2O$ (Fig. S4, ESI) which points to a quantitative Tb ⟶ Cr energy transfer we trace back to the appreciable overlap between the emitting $Tb(^5D_4)$ level and the broad Cr-centred $^4T_2 \longleftarrow {}^4A_2$ transition (Fig. 7). Since no Tb-centred emission is detected in **4**, no $Tb(^5D_4)$ lifetime is accessible and R_0(TbCr) cannot be calculated for the dipole–dipolar mechanism. However, a minimum value R_0(TbCr) ≥ 20.1 Å can be estimated from eqn. (1) when using $\eta \geq 99\%$ and $R = 9.3238$ Å (the Eu ⋯ Cr distance measured in the crystal of **7**).

Kinetic inertness of Cr^{III} in $[LnCrL_3]^{6+}$: isolation of the nonadentate receptor (HHH)-$[CrL_3]^{3+}$

Previous attempts to isolate the kinetically inert receptor (HHH)-$[CoL_3]^{3+}$ from $[LnCo^{III}L_3]^{6+}$ failed because moderately fast (within hours) isomerization processes altered the Co^{III} (d^6, low spin) coordination sphere leading to intricate mixtures of Co^{III} complexes in solution.[11] Since Cr^{III} is expected to be more inert than Co^{III} [1] and no redox M^{III}/M^{II} catalytic pathway is available (Cr^{II} is a much stronger reducing agent than Co^{II}), the decomplexation of Ln^{III} from $[LnCr^{III}L_3]^{6+}$ should provide the inert nonadentate receptor (HHH)-$[CrL_3]^{3+}$. Addition of water to 10^{-4} mol dm^{-3} solutions of $[LaCr^{III}L_3]^{6+}$ shows the disappearance of the ESI–MS peaks corresponding to $[LaCrL_3(CF_3SO_3)_i]^{(6-i)+}$ ($i = 0$–3) and the almost exclusive detection of $[CrL_3]^{3+}$ and its gas-phase adduct $[CrL_3(CF_3SO_3)]^{2+}$ for a total water concentration ≥4 mol dm^{-3} (Fig. 9a). Quantitative decomplexation of Ln^{III} in condensed phase is confirmed by the decrease of the absolute quantum yield of $[EuCr^{III}L_3]^{6+}$ (10^{-4} mol dm^{-3} in acetonitrile) with increasing water concentration, because the products $[Eu(CH_3CN)_{9-x}(H_2O)_x]^{3+}$ are non-emissive upon UV-irradiation (Fig. 9b). Finally, ^{1}H NMR spectra of $[LaCr^{III}L_3]^{6+}$ (10^{-2} mol dm^{-3} in acetonitrile) clearly show the formation of a second C_3-symmetrical species in slow exchange on the NMR time scale for water concentration in the range 1–10 mol dm^{-3}. Despite the broad signals observed for slow-relaxing Cr^{III} species, the signals of protons H [12–18] and Me [3–5] connected to the tridentate binding unit are sufficiently remote from the Cr^{III} center to limit dipolar relaxation and a reliable assignment is accessible (Table 6). For a total water concentration of 14 mol dm^{-3}, the original signals associated with $[LaCr^{III}L_3]^{6+}$ are quantitatively replaced by those of a new C_3-symmetrical complex, reminiscent of the free ligand as far as the tridentate segment is concerned (Table 6). The signals of the bidentate segments are still broad and paramagnetically shifted

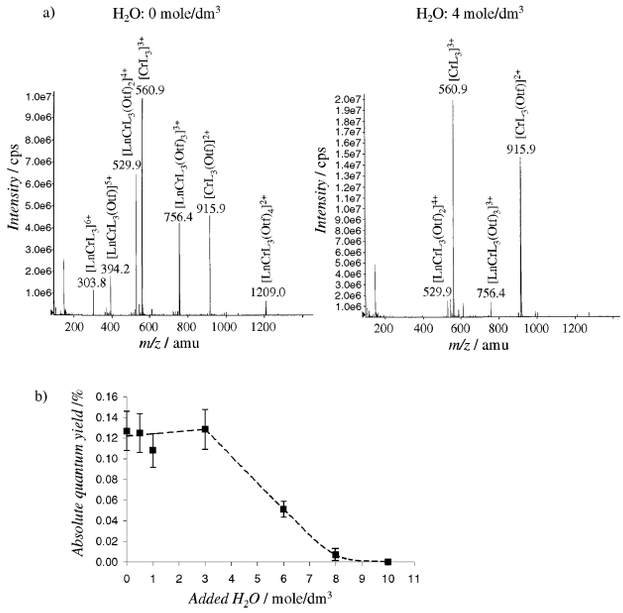

Fig. 9 Hydrolysis of (HHH)-$[LnCrL_3]^{6+}$ followed by a) ESI–MS (Ln = La, total ligand concentration 3×10^{-4} mol dm^{-3} in acetonitrile, Otf = triflate = $CF_3SO_3^-$) and b) emission spectroscopy (Ln = Eu, total ligand concentration 3×10^{-4} mol dm^{-3}, acetonitrile; the dashed line is only a guide for the eye).

in agreement with their complexation to Cr^{III} in the final hydrolysed complex. Interestingly, an identical ^{1}H NMR spectrum is obtained when $[EuCr^{III}L_3]^{6+}$ (10^{-2} mol dm^{-3} in CD_3CN) is treated with D_2O (72% v/v), thus demonstrating that the paramagnetic Eu^{III} cation has been quantitatively removed from the tridentate binding segments. Careful consideration of the ESI–MS, emission and ^{1}H NMR data shows that Ln^{III} is quantitatively extracted by water from the nine-coordinate site, thus leading to the formation of the nonadentate receptor (HHH)-$[Cr^{III}L_3]^{3+}$ as previously reported for (HHH)-$[Co^{III}L_3]^{3+}$.[11] However, no variation in the ^{1}H NMR spectrum is detected over a period of months which points to extreme kinetic inertness of (HHH)-$[Cr^{III}L_3]^{3+}$ in complete contrast with the 'fast' isomerization processes observed for the analogous Co^{III} complex.[11] Isolation on the mg scale can be achieved by treating $[LaCr^{III}L_3]^{6+}$ with $[(^nBu)_4N]_4EDTA$ in acetonitrile, followed by separation of the insoluble $[(^nBu)_4N][Ln(EDTA)]$ salt. Crystallisation in acetonitrile–diethyl ether produces a fair yield (49%) of (HHH)-$[Cr^{III}L_3](CF_3SO_3)_3\cdot 8H_2O$ (**9**) as a yellow powder. Re-dissolution in acetonitrile gives spectroscopic data identical to those observed for (HHH)-$[Cr^{III}L_3]^{3+}$ formed *in situ* by controlled hydrolysis of (HHH)-$[LnCr^{III}L_3]^{6+}$.

Conclusion

As a result of its negative reduction potential $E°([Cr(H_2O)_6]^{3+}/[Cr(H_2O)_6]^{2+}) = -0.41$ V *vs.* NHE and of its tendency to undergo inner-sphere oxidation processes, Cr^{II} is considered as a poor partner for self-assembly processes occurring in polar solvents. However, complexation with heterocyclic nitrogen donors only poorly stabilizes Cr^{II} (minor π-delocalization is detected in $[Cr(bipy)_3]^{2+}$),[19] but it destabilizes Cr^{III} to such an extent that the reduction potential shifts toward less negative values ($E°([Cr(bipy)_3]^{3+}/[Cr(bipy)_3]^{2+}) = -0.25$ V *vs.* NHE),[13] thus giving access to low-spin Cr^{II} complexes as precursors for the preparation of inert pseudo-octahedral Cr^{III} complexes. The quantitative preparation and characterization of (HHH)-$[LnCr^{II}L_3]^{5+}$ in which Cr^{II} is pseudo-octahedrally coordinated by three pyridylbenzimidazole units unambiguously demonstrates the potential of this approach. The easy oxidative post-modification process maintains the integrity of the chromium coordination sphere and this two-step self-assembly of (HHH)-

Table 6 ^{1}H NMR shifts (δ/ppm with respect to TMS) of protons connected to the tridentate binding unit in (HHH)-$[LnCr^{III}L_3]^{6+}$ (Ln = La, Eu) and (HHH)-$[CrL_3]^{3+}$ (CD_3CN, 298 K)

	(HHH)-$[LaCrL_3]^{6+}$	(HHH)-$[EuCrL_3]^{6+}$	(HHH)-$[CrL_3]^{3+}$	L [a]
H^{12}	8.60	4.80	8.43	8.38
H^{13}	8.36	6.43	8.06	7.93
H^{14}	7.84	5.51	7.59	7.57
$H^{15,16}$	2.89	2.97	3.52	3.61
$H^{17,18}$	3.38, 3.49	3.21	3.28	3.35
Me^3	4.48	3.89	4.22	4.21
Me^4	0.96	2.55	1.21	1.30
Me^5	0.78	0.45	1.03	1.13

[a] Taken from ref. 16.

$[LnCr^{III}L_3]^{6+}$ opens fascinating perspectives for the introduction of inert and spectroscopically active Cr^{III} cations into discrete supramolecular architectures whose level of organization can be controlled through a complete and reversible exploration of the energy hypersurface prior to 'kinetically fix' the final complex. Photophysical studies of $[GdCr^{III}L_3]^{6+}$ point to classical Cr^{III}-centred spectroscopic properties resulting from spin-allowed d–d and CT transitions together with long-lived luminescence of the $Cr(^2E)$ level. For $[LnCr^{III}L_3]^{6+}$ (Ln = Eu, Tb), intramolecular intermetallic Ln $\longrightarrow$ Cr^{III} energy transfer processes strongly affect the Ln-centred photophysical properties which can be modulated by the nature of the intermetallic communication. Treatment of our data with the simple dipole–dipole model shows that the critical radius for 50% energy transfer for the Eu/Cr pair amounts to $R_0 \approx 10.8$ Å while the better resonance conditions found for the Tb/Cr pair extends this value to $R_0 \geq 20.1$ Å. This remarkable increase may find applications for probing biological structures which require long-range energy transfer processes.[39] Attempts to use Cr^{III} as a donor for sensitizing Tm^{III} emission as observed in Al_2O_3 garnets[8] failed because of the poor energy match between $Cr(^2E)$ and $Tm(^3F_{2,3})$ levels which is not compensated by overlap with the broader $Cr(^4T_2)$ level lying at too high energy in $[TmCr^{III}L_3]^{6+}$. Finally, decomplexation of Ln^{III} *via* competition with water or $EDTA^{4-}$ provides the first nonadentate C_3-symmetrical receptor possessing an optically active Cr^{III} tripod; a classical template method has been recently reported for the preparation of a related hexadentate receptor.[40] The extreme inertness of the latter tripod is currently investigated for performing chiral resolution of lanthanide-containing triple-helical complexes.

Experimental

Solvents and starting materials

These were purchased from Fluka AG (Buchs, Switzerland) and used without further purification unless otherwise stated. The ligand 2-{6-[*N*,*N*-diethylcarboxamido]pyridin-2-yl}-1,1′-dimethyl-5,5′-methylene-2′-(5-methylpyridin-2-yl)bis[1H-benzimidazole] (L) was prepared according to literature procedures.[16] The triflate salts $Ln(CF_3SO_3)_3{\cdot}nH_2O$ (Ln = La–Lu, Y) were prepared from the corresponding oxides (Rhodia, 99.99%).[41]

Preparation of $[Cr(CF_3SO_3)_2]{\cdot}13H_2O$

A solution of 80 mmol of trifluoromethanesulfonic acid (7 cm^3) in degassed water (50 cm^3) at 0 °C was added *via* a cannula to electrolytic chromium (2 g, 38 mmol) under nitrogen. After stirring for 24 h at 60 °C, the blue solution was filtered and evaporated to dryness. The resulting blue powder was dried under vaccum (10^{-2} Torr/24 h) and transferred into a glove box. Spectrophotometric analysis of the chromium content after oxidation into chromate (fusion with KNO_3) gives %Cr = 8.87 corresponding to $[Cr(CF_3SO_3)_2]{\cdot}13H_2O$ (%Cr = 8.90).

Preparation of $[LnCr^{III}L_3](CF_3SO_3)_6{\cdot}mH_2O$ (Ln = La, *m* = 2: 1; Ln = Eu, *m* = 4: 2; Ln = Gd, *m* = 6: 3; Ln = Tb, *m* = 3: 4; Ln = Tm, *m* = 4: 5; Ln = Lu, *m* = 2: 6)

A solution of 18 μmol of $Ln(CF_3SO_3)_3{\cdot}nH_2O$ (Ln = La, Eu, Gd, Tb, Tm, Lu) in acetonitrile (2 cm^3) was slowly added to a solution of L (30 mg, 54 μmol) in 1 : 1 CH_2Cl_2 : CH_3CN (4 cm^3). After stirring for 10 min at room temperature, the solution was evaporated, the solid residue dried under vacuum and redissolved in degassed CH_3CN (3 cm^3) in the glove box. A solution of 18 μmol of $[Cr(CF_3SO_3)_2]{\cdot}13H_2O$ (10.8 mg) in degassed acetonitrile (1 cm^3) was slowly added and the deep green mixture was stirred for 1 h. Tetrabutylammonium triflate (18 μmol, 7.2 mg) was added in one portion and air was slowly diffused for one hour into the solution. The resulting yellow mixture was evaporated to dryness and the solid residue dissolved in acetonitrile (0.5 cm^3). Fractional crystallisation with diethyl ether produced yellow microcrystals after separation of a waxy brown precipitate. The resulting yellow microcrystalline aggregates were collected by filtration and dried to give 33–68% of complexes $[LnCr^{III}L_3](CF_3SO_3)_6{\cdot}mH_2O$ (Ln = La, *m* = 2: **1**; Ln = Eu, *m* = 4: **2**; Ln = Gd, *m* = 6: **3**; Ln = Tb, *m* = 3: **4**; Ln = Tm, *m* = 4: **5**; Ln = Lu, *m* = 2: **6**). Complexes **1**–**6** were characterized by their IR spectra and gave satisfactory elemental analyses (Table S2, ESI). X-Ray quality prisms of **7** and **8** were obtained by slow diffusion of diethyl ether into concentrated acetonitrile solutions of **2** (Ln = Eu) and **6** (Ln = Lu), respectively.

Preparation of $[CrL_3](CF_3SO_3)_3{\cdot}8H_2O$ (9)

A solution of 12 μmol of $[(^nBu)_4N]_4EDTA{\cdot}6.4H_2O$ in acetonitrile (135 μl) was added to a solution of $[LaCrL_3](CF_3SO_3)_6(H_2O)_2$ (**2**, 35.1 mg, 12 μmol) in acetonitrile (1 ml). The resulting white precipitate ($[(^nBu)_4N][La(EDTA)]$) was removed by centrifugation and the remaining clear solution concentrated. Diethyl ether was allowed to diffuse during 2 d and the orange oil was freezed at −20 °C for 2 h. Subsequent ultrasonic treatment induced precipitation. The separated solid was dissolved in acetonitrile/HCl 10^{-3} mol dm^{-3} (0.3 cm^3/0.3 cm^3) and loaded on a cellulose column. Elution with aqueous HCl (0 $\longrightarrow$ 10^{-3} mol dm^{-3}) followed by evaporation of the solvent and precipitation according to the standard work up process (*vide infra*) yielded 5.9 μmol of $[CrL_3](CF_3SO_3)_3{\cdot}8H_2O$ (**9**) as an orange powder (14.9 mg, 49%).

Crystal structure determination of $[LnCrL_3](CF_3SO_3)_6(CH_3CN)_4$ (Ln = Eu, 7; Ln = Lu, 8)

A summary of the crystal data, intensity measurements and structure refinements are reported in Table 7. Data were corrected for LP effects and for absorption. The structures were solved by direct methods using MULTAN 87;[42] all other calculations used XTAL[43] and ORTEP II[44] programs. The hydrogen atoms of the methyl groups were refined with restraints on bond distances and bond angles and blocked during the last cycles. The other H-atoms were placed in calculated positions and contributed to F_c calculations. For **7**, the methyl C30b and

Table 7 Summary of crystal data, intensity measurements and structure refinement for $[LnCr^{III}L_3](CF_3SO_3)_6(CH_3CN)_4$ (Ln = Eu, **7**; Ln = Lu, **8**)

	7	**8**
Formula	$EuCrC_{113}H_{111}N_{25}O_{21}F_{18}S_6$	$LuCrC_{113}H_{111}N_{25}O_{21}F_{18}S_6$
Molecular weight	2893.6	2916.6
Color	Yellow	Yellow
Crystal system	Monoclinic	Monoclinic
Space group	$P2_1/n$	$P2_1/n$
a/Å	22.2803(9)	22.2939(13)
b/Å	22.9088(11)	22.9355(9)
c/Å	24.6170(11)	24.3903(15)
β/°	92.216(5)	92.258(7)
V/Å^3	12555(1)	12462(1)
Z	4	4
μ(Mo-Kα)/mm^{-1}	0.79	1.08
Temperature/K	200	200
Reflections measured	104136	134595
Reflections unique	24370	24244
Reflections observed ($\|F_o\| > 4\,\sigma(F_o)$)	11'858	14'416
R	0.038	0.040
R_w	0.037	0.040

the triflate anion *i* were disordered and refined on two different sites and population parameters of 0.7/0.3 and 0.75/0.25 respectively. The disordered atomic sites displaying larger population parameters were refined with anisotropic displacement parameters and those corresponding to the smaller population parameters with isotropic displacement parameters.

CCDC reference numbers 176855 and 176856.

See http://www.rsc.org/suppdata/dt/b2/b200011c/ for crystallographic data in CIF or other electronic format.

Spectroscopic measurements

Electronic spectra in the UV–Vis were recorded at 20 °C from 10^{-3} mol dm^{-3} solutions in MeCN with a Perkin-Elmer Lambda 900 spectrometer using quartz cells of 0.1 and 0.01 cm path length. IR spectra were obtained from KBr pellets with a Perkin-Elmer 883 spectrometer. ^{1}H NMR spectra were recorded at 25 °C on a Broadband Varian Gemini 300 spectrometer. Chemical shifts are given in ppm *vs*. TMS. Pneumatically-assisted electrospray (ESI–MS) mass spectra were recorded from 10^{-4} mol dm^{-3} acetonitrile solutions on API III and API 365 tandem mass spectrometers (PE Sciex) by infusion at 4–10 µl min^{-1}. The spectra were recorded under low up-front declustering or collision induced dissociation (CID) conditions, typically ΔV = 0–30 V between the orifice and the first quadrupole of the spectrometer. The experimental procedures for high-resolution, laser-excited luminescence measurements have been published previously.[45] Solid state samples were finely powdered and low-temperature (295–10 K) was achieved by means of a Cryodyne Model 22 closed-cycle refrigerator from CTI Cryogenics. Luminescence spectra were corrected for the instrumental function, but not excitation spectra. Lifetimes are averages of at least 3–5 independent determinations and were measured using excitation provided by a Quantum Brillant Nd:YAG laser equipped with frequency doubler, tripler and quadrupler as well as with an OPOTEK *Magic*Prism™ OPO crystal. Ligand excitation and emission spectra, as well as quantum yields were recorded on a Perkin-Elmer LS-50B spectrometer equipped for low-temperature measurements. The quantum yields Φ have been calculated using the equation $\Phi_x/\Phi_r = A_r(\tilde{\nu})I_r(\tilde{\nu})n_x^2D_x/A_x(\tilde{\nu})I_x(\tilde{\nu})n_r^2D_r$, where x refers to the sample and r to the reference; A is the absorbance, $\tilde{\nu}$ the excitation wavenumber used, I the intensity of the excitation light at this energy, n the refractive index and D the integrated emitted intensity. $[Eu(terpy)_3](ClO_4)_3$ (Φ = 1.3%, acetonitrile, 10^{-3} mol dm^{-3}) and $[Tb(terpy)_3](ClO_4)_3$ (Φ = 4.7%, acetonitrile, 10^{-3} mol dm^{-3}) were used as references for the determination of quantum yields of respectively Eu- and Tb-containing samples.[29,46] Elemental analyses were performed by Dr H. Eder from the microchemical Laboratory of the University of Geneva.

Acknowledgements

This work is supported through grants from the Swiss National Science Foundation. We thank Frédéric Gumy for his help in measuring the luminescence spectra and lifetimes and Prof. Andreas Hauser for fruitful discussions.

References

1 S. F. Lincoln and A. E. Merbach, *Adv. Inorg. Chem.*, 1995, **42**, 1.
2 A. B. P. Lever, *Electronic Spectroscopy*, 2nd edn., Elsevier, Amsterdam, 1984, 417.
3 S. Decurtins, M. Gross, H. W. Schmalle and S. Ferlay, *Inorg. Chem.*, 1998, **37**, 2443; R. Sieber, S. Decurtins, H. Stoeckli-Evans, C. Wilson, D. Yufit, J. A. K. Howard, S. C. Capelli and A. Hauser, *Chem. Eur. J.*, 2000, **6**, 361.
4 T. Sanada, T. Suzuki, T. Yoshida and S. Kaizaki, *Inorg. Chem.*, 1998, **37**, 4712; M. A. Subhan, T. Suzuki and S. Kaizaki, *J. Chem. Soc., Dalton Trans.*, 2001, 492.
5 X. Zhang, Y. Cui, F. Zheng and J. Huang, *Chem. Lett.*, 1999, 1111.
6 D. Burdinski, F. Birkelbach, T. Weyermüller, U. Flörke, H.-J. Haupt, M. Lengen, A. X. Trautwein, E. Bill, K. Wieghardt and P. Chaudhuri, *Inorg. Chem.*, 1998, **37**, 1009.
7 N. Serpone and M. Z. Hoffmann, *J. Chem. Educ.*, 1983, **60**, 853; A. D. Kirk, *Chem. Rev.*, 1999, **99**, 1607.
8 Y. Shen, T. Riedener and K. L. Bray, *Phys. Rev. B*, 2000, **61**, 11460.
9 P. A. Brayshaw, J.-C. G. Bünzli, P. Froidevaux, J. M. Harrowfield, Y. Kim and A. N. Sobolev, *Inorg. Chem.*, 1995, **34**, 2068.
10 J.-M. Lehn, *Chem. Eur. J.*, 1999, **5**, 2455; C. Piguet, *J. Inclusion Phenom. Macrocycl. Chem.*, 1999, **34**, 361.
11 S. Rigault, C. Piguet, G. Bernardinelli and G. Hopfgartner, *Angew. Chem., Int. Ed.*, 1998, **37**, 169; S. Rigault, C. Piguet, G. Bernardinelli and G. Hopfgartner, *J. Chem. Soc., Dalton Trans.*, 2000, 4587.
12 L. Chong and R. B. Jordan, *Inorg. Chem.*, 1987, **26**, 3855.
13 B. R. Baker and B. D. Mehta, *Inorg. Chem.*, 1965, **4**, 848.
14 E. König and S. Herzog, *J. Inorg. Nucl. Chem.*, 1970, **32**, 585.
15 B. de Castro and C. Freire, *Synth. React. Inorg. Met.-Org. Chem.*, 1990, **20**, 1.
16 C. Piguet, J.-C. G. Bünzli, G. Bernardinelli, G. Hopfgartner, S. Petoud and O. Schaad, *J. Am. Chem. Soc.*, 1996, **118**, 6681.
17 C. Piguet, E. Rivara-Minten, G. Bernardinelli, J.-C. G. Bünzli and G. Hopfgartner, *J. Chem. Soc., Dalton Trans.*, 1997, 421; C. Edder, C. Piguet, G. Bernardinelli, J. Mareda, C. G. Bochet, J.-C. G. Bünzli and G. Hopfgartner, *Inorg. Chem.*, 2000, **39**, 5059.
18 G. N. La Mar and G. R. van Hecke, *J. Chem. Phys.*, 1970, **52**, 5676.
19 G. N. La Mar and G. R. van Hecke, *J. Am. Chem. Soc.*, 1969, **91**, 3442.
20 I. Bertini and C. Luchinat, *Coord. Chem. Rev.*, 1996, **150**, 77.
21 T. Schönherr, M. Atanasov and A. Hauser, *Inorg. Chem.*, 1996, **35**, 2077.
22 G. Hopfgartner, C. Piguet and J. D. Henion, *J. Am. Soc. Mass Spectrom.*, 1994, **5**, 748.
23 J.-L. Pascal and M. E. M. Hamidi, *Polyhedron*, 1994, **13**, 1787.
24 R. D. Shannon, *Acta Crystallogr., Sect. A*, 1976, **32**, 751.

25 A. Hauser, M. Mäder, W. T. Robinson, R. Murugesan and J. Ferguson, *Inorg. Chem.*, 1987, **26**, 1331; K. V. Goodwin, W. T. Pennington and J. D. Petersen, *Inorg. Chem.*, 1989, **28**, 2016.
26 C. Piguet, G. Bernardinelli, B. Bocquet, O. Schaad and A. F. Williams, *Inorg. Chem.*, 1994, **33**, 4112.
27 M. Meyer, B. Kersting, R. E. Powers and K. N. Raymond, *Inorg. Chem.*, 1997, **36**, 5179.
28 J. H. Brewster, *Top. Curr. Chem.*, 1974, **47**, 29; F. Renaud, C. Piguet, G. Bernardinelli, J.-C. G. Bünzli and G. Hopfgartner, *J. Am. Chem. Soc.*, 1999, **121**, 9326.
29 S. Petoud, J.-C. G. Bünzli, C. Piguet, Q. Xiang and R. Thummel, *J. Luminesc.*, 1999, **82**, 69.
30 W. T. Carnall, P. R. Fields and K. Rajnak, *J. Chem. Phys.*, 1968, **49**, 4443.
31 V. S. Langford, M. E. von Arx and A. Hauser, *J. Phys. Chem. A*, 1999, **103**, 7161.
32 D. L. Dexter, *J. Chem. Phys.*, 1953, **21**, 836; B. Schlicke, P. Belser, L. De Cola, E. Sabbioni and V. Balzani, *J. Am. Chem. Soc.*, 1999, **121**, 4207.
33 T. Förster, *Ann. Phys.*, 1948, 55; T. Förster, *Discuss. Faraday Soc.*, 1959, **27**, 7.
34 S. T. Frey and W. W. Horrocks, *Inorg. Chim. Acta*, 1995, **229**, 383.
35 J.-C. G. Bünzli, in *Lanthanide Probes in Life, Chemical and Earth Sciences*, eds. J.-C. G. Bünzli and G. R. Choppin, Elsevier, Amsterdam, 1989, ch. 7.
36 C. Piguet, J.-C. G. Bünzli, G. Bernardinelli, G. Hopfgartner and A. F. Williams, *J. Am. Chem. Soc.*, 1993, **115**, 8197; M. Elhabiri, R. Scopelliti, J.-C. G. Bünzli and C. Piguet, *J. Am. Chem. Soc.*, 1999, **121**, 10747.
37 C. Edder, C. Piguet, J.-C. G. Bünzli and G. Hopfgartner, *J. Chem. Soc., Dalton Trans.*, 1997, 4657; C. Edder, C. Piguet, J.-C. G. Bünzli and G. Hopfgartner, *Chem. Eur. J.*, 2001, **7**, 3014.
38 F. S. Richardson, D. H. Metcalf and D. P. Glover, *J. Phys. Chem.*, 1991, **95**, 6249 and references therein.
39 I. M. Clarkson, A. Beeby, J. I. Bruce, L. J. Govenlock, M. P. Lowe, C. E. Mathieu, D. Parker and K. Senanayake, *New J. Chem.*, 2000, **24**, 377; M. Li and P. R. Selvin, *J. Am. Chem. Soc.*, 1995, **117**, 8132.
40 H. Weizman, J. Libman and A. Shanzer, *J. Am. Chem. Soc.*, 1998, **120**, 2188.
41 J. F. Desreux, in *Lanthanide Probes in Life, Chemical and Earth Sciences*, eds. J.-C. G. Bünzli and G. R. Choppin, Elsevier, Amsterdam, 1989, ch. 2, p. 43.
42 P. Main, S. J. Fiske, S. E. Hull, J. Lessinger, D. Germain, J.-P. Declercq and M. M. Woolfson, MULTAN 87, Universities of York, England and Louvain-La-Neuve, Belgium, 1987.
43 XTAL 3.2 User's Manual, eds. S. R. Hall, H. D. Flack, J. M. Stewart, Universities of Western Australia and Maryland, 1989.
44 C. K. Johnson, ORTEP II, Report ORNL-5138, Oak Ridge National Laboratory: Oak Ridge, Tennessee, 1976.
45 C. Piguet, A. F. Williams, G. Bernardinelli, E. Moret and J.-C. G. Bünzli, *Helv. Chim. Acta*, 1992, **75**, 1697; P. Guerriero, P. A. Vigato, J.-C. G. Bünzli and E. Moret, *J. Chem. Soc., Dalton Trans.*, 1990, 647.
46 C. Piguet, J.-C. G. Bünzli, G. Bernardinelli, C. G. Bochet and P. Froidevaux, *J. Chem. Soc., Dalton Trans.*, 1995, 83.